SHARK-NIR system design analysis overview

Valentina Viotto*[a,b], Jacopo Farinato[a,b], Davide Greggio[a,b,c], Daniele Vassallo[a,b,c], Elena Carolo[a,b], Andrea Baruffolo[a], Maria Bergomi[a,b], Alexis Carlotti[d], Marco De Pascale[a], Valentina D'Orazi[a,b], Daniela Fantinel[a], Demetrio Magrin[a,b], Luca Marafatto[a,b], Lars Mohr[e], Roberto Ragazzoni[a,b], Bernardo Salasnich[a], Christophe Verinaud[d]

[a]INAF – Osservatorio Astronomico di Padova, Vicolo dell'Osservatorio 5, 35122, Padova, Italy;
[b]ADONI - Laboratorio Nazionale Ottiche Adattive, Italy;
[c]Dipartimento di Fisica e Astronomia, Università degli Studi di Padova, Vicolo dell'Osservatorio 3, 35122, Padova, Italy;
[d]Institut de Planétologie et d'Astrophysique de Grenoble, 414, Rue de la Piscine, Domaine Universitaire, 38400 St-Martin d'Hères, France;
[e]Max-Planck-Institut für Astronomie, Königstuhl 17 D-69117 Heidelberg, Germany

ABSTRACT

In this paper, we present an overview of the System Design Analysis carried on for SHARK-NIR, the coronagraphic camera designed to take advantage of the outstanding performance that can be obtained with the FLAO facility at the LBT, in the near infrared regime. Born as a fast-track project, the system now foresees both coronagraphic direct imaging and spectroscopic observing mode, together with a first order wavefront correction tool. The analysis we here report includes several trade-offs for the selection of the baseline design, in terms of optical and mechanical engineering, and the choice of the coronagraphic techniques to be implemented, to satisfy both the main scientific drivers and the technical requirements set at the level of the telescope. Further care has been taken on the possible exploitation of the synergy with other LBT instrumentation, like LBTI. A set of system specifications is then flown down from the upper level requirements to finally ensure the fulfillment of the science drivers. The preliminary performance budgets are presented, both in terms of the main optical planes stability and of the image quality, including the contributions of the main error sources in different observing modes.

Keywords: Coronagraphy, Adaptive Optics

1. INTRODUCTION

SHARK (System for coronagraphy with High order Adaptive optics from R to K band) is an instrument proposed for the LBT[1] in the framework of the "2014 Call for Proposals for Instrument Upgrades and New Instruments". It is composed by two channels, a visible and a near infrared arm, to be installed one for each LBT telescope, and it will exploit, in its binocular fashion, unique challenging science from exoplanet to extragalactic topics with simultaneous spectral coverage from R to H band, taking advantage of the outstanding performances of FLAO[2], the Pyramid Wavefront Sensor[3] (P-WFS) based Adaptive Optics (AO) module. This paper includes the main trades-off for the selection of SHARK-NIR baseline opto-mechanical design presented at the Conceptual Design Review, fully described in [4]. A summary of the identified critical issues is also given, with possible solutions and compensators.

2. CONCEPTUAL DESIGN TRADE-OFF

During the Conceptual Design Phase, the design of SHARK-NIR underwent some major changes with respect to what previously presented[5]. These changes are the results of different trades-off which are described in the following.

* valentina.viotto@oapd.inaf.it

Modeling, Systems Engineering, and Project Management for Astronomy VI,
edited by George Z. Angeli, Philippe Dierickx, Proc. of SPIE Vol. 9911, 991127
 · doi: 10.1117/12.2232757

2.1 Instrument scientific wavelengths

Originally, SHARK-NIR was supposed to be optimized from J to K band. This would obviously have implied the use of a cryostat, to maintain the full optical train of the instrument at a low temperature, in order to minimize the thermal background. This necessity would translate into further needs. First of all, the whole optical design was required to be as compact as possible, and this did not allow to implement several coronagraphic techniques with different requirements (e.g. the presence of an intermediate pupil plane). Moreover, to minimize the stress between the various opto-mechanical components, when going from ambient to operating temperature, the fully reflective design was foreseen to be implemented using aluminum optics, in order to keep the same CTE of the mechanics. On the other hand, aluminum optics, despite being light and suitable for cryogenic systems, can be machined only up to a certain level of micro-roughness, limiting the nominal performance of the full optical train. The current baseline for SHARK-NIR foresees a wavelength range from J to H band[4].Of course, to give up the K band has its drawbacks in the science that can be performed with the instrument itself. A comparison of the achievable contrast, for the classical Lyot technique[6], in H and K band has been made. The contrast loss by giving up the K-band is about a factor two in bad seeing conditions, while it is of the order of 25% in good seeing conditions, and it is expected to be largely compensated by using more efficient coronagraphic techniques.

In the exoplanet science it is needed to exploit photometric techniques in different bands in order to build up the spectral energy distribution of sub-stellar objects and to define the L/T transition (for example in the colour-magnitude plane J vs J-H[7]). The more extended is the spectral coverage, the better we can characterize the exoplanet properties. The counterpart to the H-band observation with SHARK-NIR can come from L' coronagraphic observations carried on with LBTI[8]. On the other hand, other scientific cases need to obtain data from molecolar oxigen lines, the strongest of which are in the K band. Also in this framework, an agreement with the LBTI group is under definition, with the goal to exploit the synergy with a coronagraph working in the K band on LMIRcam[9]. Details of the possible synergy between instruments mounted at the LBT are reported in [4].

2.2 The scientific Field of View size

A trade-off, which included the scientific Field of View size, has been carried on, alternatively using either only one quadrant (S-FoV) or a full 2Kx2K (L-FoV) H1RG Teledyne infrared detector.

Table 1. Main parameters of the two different FoV designs.

Parameter	S-FoV design	L-FoV design
Detector format [px]	1024	2048
FoV size ["]	15.3	30.67
FoV along the diagonal ["]	21.64	43.37
Scale ["/px]	0.015	0.015
Nyquist sampling at [μm]	1.00	1.00

As can be seen in Table 1, the two considered scientific FoV sizes are slightly more than 15"x15" and 30"x30", respectively. The main driver of the large FoV (L-FoV) design was the goal to become more attractive also in the instrument direct imaging observing mode. This necessity arose from the lack of a high quality imaging camera for the LBT, which could take fully advantage of the Adaptive Optics correction delivered by FLAO. More recent information about LBT instruments upgrades and readiness level tell us that this will not be a real issue at the time when SHARK-NIR could be commissioned. On the other hand, going back to the small FoV (S-FoV) approach (now updated with respect to the one proposed in the past[5]) gives us some advantages. First of all, it is possible to use a "leftover chip", meaning a Teledyne 2Kx2K chip, which could not be used in another instrument because part of it shows some problems or, in general, don't work properly. If a chip like this could be found, in addition to buy a cheaper item, we would also probably save some time, which is a key point for this project. Secondarily, being the direct imager not a priority anymore, and since no coronagraphic science case needs a wide field of view, we keep the possibility to exploit the imaging performance of FLAO in the NIR band, only for the science cases which really need a very high Strehl Ratio (SR) (which, on the other hand, rarely require a wide field too).

2.3 The intermediate pupil

Given the choice of optimizing the design for a shorter bandwidth (which does not require cold optics) and for a smaller FoV, we can take advantage of the saved space (given the envelope allowed by the telescope interface) to increase the complexity of the optical design. This is particularly interesting in the view of introducing an intermediate pupil plane. This, of course, requires an increase in the number of optical elements in the design, which has also the drawback to slightly decrease the total throughput. This throughput loss can be estimated comparing the number of reflecting surfaces in the two designs. The original design presented in [5] included 2 Off-Axis Parabolas (OAPs) and 3 folding mirrors, while a design which also reimages an intermediate pupil plane includes 4 OAPs, 3 folding mirrors and a Tip-Tilt (TT) mirror, which means an increase of 3 reflections. If we only consider the mirrors contributions (neglecting Atmospheric Dispersion Correction – ADC - , masks and filters, for the moment), assuming a conservative 98% reflectivity for each mirror, this would reduce the overall throughput of about 5%. On the other hand, the bandpass cutoff change (from K to H) relaxes the requirements on the thermal behavior of the opto-mechanical design, since the thermal range is reduced a lot, not being the full optical train cryogenic anymore. As we already mentioned, then, glass mirrors (instead of the previously foreseen Aluminum ones) can be used, and this choice could improve the performance of the system in terms of scattered light (lower microroughness).

The huge advantage of a design in which the pupil plane is reimaged is the flexibility of the overall system to the implementation of different and more sophisticated coronagraphic designs, already implemented in other planet finders (e.g. GPI[10] and SPHERE[11]), like the Apodized Lyot[12] or the Shaped Pupil[13] coronagraphs.

3. CRITICAL ISSUES

We have identified what we believe are the most important critical issues, and we briefly describe what is the plan to properly address them.

3.1 Tracking of the PSF movements

As a possible way to monitor movements of the Point Spread Function (PSF), in the current design a TT sensor has been added to the optical train, picking up part of the light (few %) of the central star with a beam splitter. The WFS will be coupled with the local TT mirror. The possibility to implement, in the future, a low order WFS and to substitute the TT mirror with a local Deformable Mirror, to correct for non-common path aberrations (Section 3.3), is kept open. The sensitivity with which the system will be able to measure (and then correct) the PSF movements on the focal plane is driven by the quality and sampling of the PSF on the TT camera. Most of the light of the spot on that camera will be included in ~10 pixels. According with previous experience in computing stable centroids with a simple routine on spots of about 10 pixel in diameter, we assume we will be easily sensitive to shifts of the spot of ½ pixel~5mas.

3.1.1 Long term drift

Changes in the opto-mechanical setup during the exposure (due to flexures, thermal reasons, etc.) can cause misalignments in the masks positioning which can drop quickly the system performance; one way to track the flexures is to follow the PSF movements during the exposure. For the planet finding with Angular Differential Imaging[14] (ADI) mode, during exposure the telescope elevation is almost blocked, since the observation is carried on when the target is close to meridian. In the same configuration, the mechanical de-rotator used to rotate the whole SHARK-NIR system is blocked too. For these reasons, we do not expect large flexures with this operational mode. In any case, it's safer to have a way to monitor long term drifts during exposure and it becomes mandatory for the other scientific case and operational modes, in which the system de-rotates and the telescope changes its elevation during the exposure. In the current design, being it updated in a way that an intermediate focal plane exists, we can consider some options to perform this operation. In the current design of the system, in fact, the focused light coming from the LBT arm, and picked up to feed SHARK-NIR, is re-imaged into three focal planes:

- a folded one, in which some the light is picked up by a beam splitter, to feed the TT sensor.
- an intermediate focal plane (in between the two pupil planes), where the occulting mask is positioned.
- the final focal plane, where the scientific image is retrieved by the IR-camera.

This means that there are two focal planes which can be monitored using a detector, but no way to compensate for displacements of the PSF occurring in the non-common path between the two of them. Being compactness and stability

two of the drivers of the full system opto-mechanical design, we do not expect flexures internal to the instrument to play a major role. This, of course, shall be verified, monitoring, for different orientations of SHARK-NIR with respect to the gravity vector, the movement of a focused image on the two detectors.

Once the instrument will be installed on the telescope, a characterization of the flexures and of their effect on the PSF stability will be mandatory. If a relative shift of the PSF in the folded and the final focal planes is not identified, meaning that no internal flexures occur, then the spot can be centered with respect to the occulting masks filter wheels, minimizing the light reaching the scientific NIR camera, once a calibrated occulting mask is positioned into the optical path. Then, the position of the PSF on the folded focal plane can be retrieved to act as a reference for the centering operations in between exposures. On the contrary, if a relative shift of the PSF in the folded and the final focal planes is identified, instead, it will be necessary to extend the characterization with a look-up table. That shall report, for each elevation angle and de-rotator position, the pixel on the folded focal plane TT camera, where the focused spot lays when the occulting mask centering is optimized (again, looking at the residual light reaching the scientific camera). It is possible that the spot position does not change on the TT camera, internal flexures only occur after the intermediate focal plane. This is likely to be true, being the most of the optics and mounts placed in that area. Whatever the way to retrieve the drift, PSF movements may be fed then back to the telescope pointing system or to the local TT mirror to correct for them.

3.1.2 AO correction residual jitter

The LBT, like all the large telescopes, suffers from structure vibrations that can reduce the AO performance. These vibrations are due to the swing arm supporting the Adaptive Secondary Mirror[15] (ASM) resonance frequencies, excited by wind shaking and tracking. Additional vibrations con come from other sources, like the cooling system. The main modes affected by these vibrations are the lowest, i.e. the tip and tilt. During the commissioning of FLAO, the FLAO team characterized these vibrations in open loop and identified the telescope vibration peak at ~13 Hz (FLAO commissioning report). Some of these effects can be corrected by the AO system. The residual vibration spectrum was also characterized during the FLAO commissioning, both on the P-WFS and on the InfraRed Test Camera. Obviously, we are interested on the amplitude of this vibration, because it shall affect the occulting masks design. During FLAO commissioning, a residual TT power rms on the vibration at 13.4Hz, estimated from TT residual modes, was computed versus the equivalent estimation using the PSF images. The spread of the measurements covers the range between 1 and 12 milliarcseconds, and its median value lies at about 7-8mas. At the moment, we are taking this value into consideration, in the design of the pupil and focal plane masks and in the selection of coronagraphic techniques to be implemented. It is still possible, however, that this jitter is reduced in the future. First of all, the part of this noise, which is coming from the FLAO loop digital controller, is being investigated and the situation could improve with the foreseen upgrade of the AO facility into SOUL[16]. Another possibility for a future upgrade of SHARK-NIR, is to use the beam splitter to pick-up more than only few percents of the light entering the instrument, and close an internal TT AO loop with the local TT mirror, during exposure.

3.2 Tracking of the pupil movements

The telescope pupil image movements with respect to the SKARK-IR interface, occurring during an exposure, shall be estimated and, in case, corrected, since they could kill the coronagraphic performance moving the star away from the occulting mask. A preliminary discussion with the ASM team is giving possible displacements, at the level of the adaptive secondary mirror (that, we recall, at LBT is defining the pupil) of the order of a few millimeters (3-4mm) while pointing in every direction on sky (private communication). This corresponds to a movement of about 0.4% of the pupil. The pupil movements during a single exposure have not been characterized, however, given the peculiar kind of exposure, which are foreseen for the exoplanet scientific case (on-meridian exposures, to take advantage of ADI for the data reduction), the telescope elevation shall not change a lot during a single exposure. Because of that, flexures are expected to be by far lower than the ones one could measure randomly pointing at the whole sky. In the current design, nothing is foreseen to look at the pupil movements during a single exposure. An analysis has been performed to verify the effect on the contrast degradation of a shift of the pupil mask with respect to the pupil image during an exposure. Results show that for shifts lower than 1% the effect is negligible for all the masks implemented in the simulations[17].

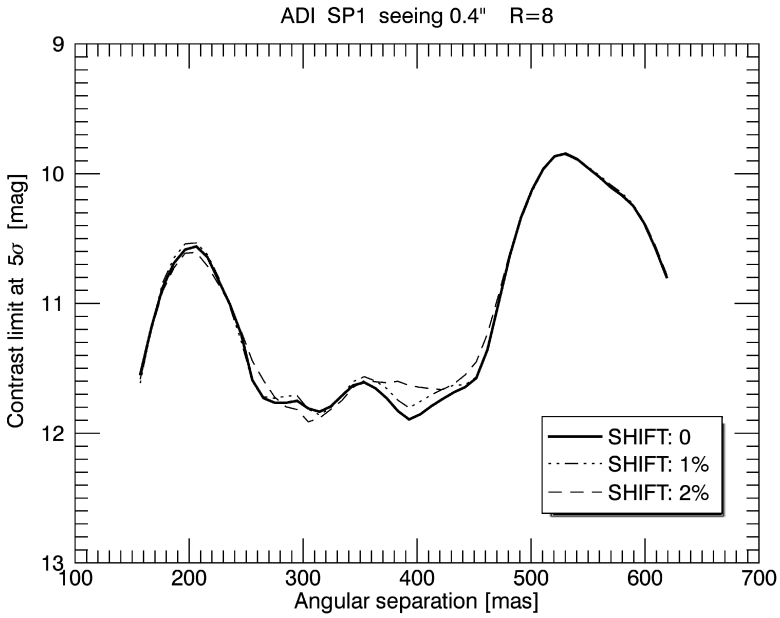

Figure 1 comparison of the contrast limit which can be reached for different pupil image shift, in the case of a Shaped Pupil coronagraph (the most sensitive to pupil shift we have considered)

On the other hand, pupil movements between the exposures shall be monitored and, in case, the pupil re-centered on the pupil mask to fulfill the requirements of the coronagraphic techniques implemented. The tolerance on the pupil positioning on the mask and its stability during a single exposure depends on the kind of coronagraph implemented and on the design of the mask itself. At the moment, we are using masks with a tolerance of about 1% for the shaped pupil. With this aim, SHARK-NIR design, has been equipped with a deployable doublet, to be inserted into the optical path to re-image the pupil onto the detector. This will allow to adjust the pupil position before the exposure, in order to center the pupil image onto the calibrated reference on the detector. The size of the re-imaged pupil is ≈7.1 mm and it is sampled by the scientific camera with approximately 390 pixels. However, the optical quality of the image is dependent on the zenith angle of observation and can be worse than the pixel size, leading to a smaller effective sampling. This pupil image, in fact, suffers from a chromatic aberration generated by the ADC, due to the fact that the ADC is not placed in a pupil plane and so it is correcting the angles of the rays in a plane far from the pupil.

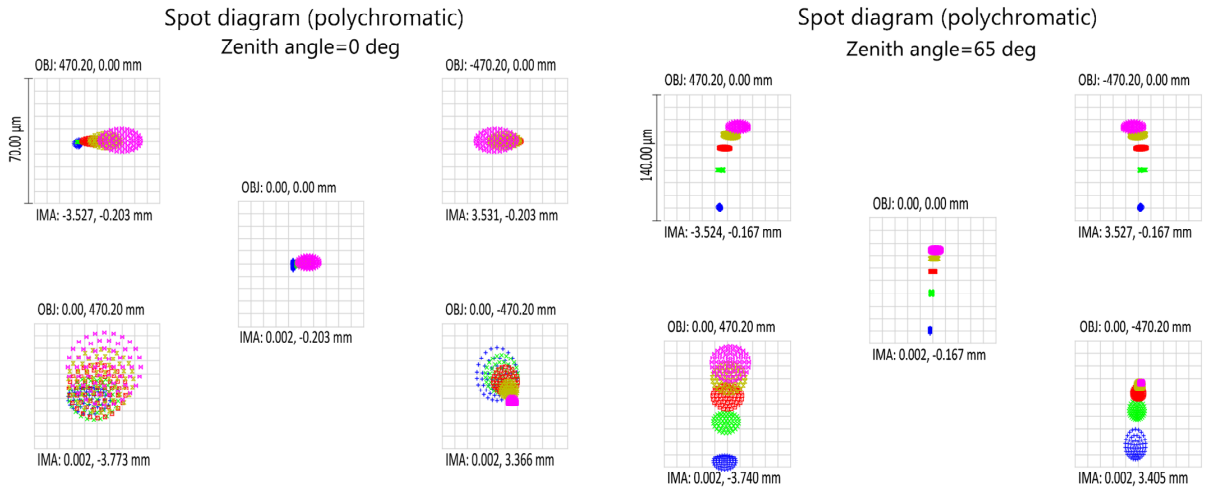

Figure 2 Spot diagram for the pupil image on the scientific detector (for the full bandwidth) when using the ADC to correct atmospheric dispersion at ZA=0deg (left) and ZA=65deg (right).

This results in a chromatic dispersion on the pupil planes placed after the ADC in the optical path. The amount of dispersion depends on the distance between the ADC and the pupil image and on the zenithal angle. Figure 5 shows the dispersion effect for the full bandwidth for ZA=0deg and ZA=65 deg. In the worst case (ZA=65deg) the dispersion is smaller than 140μm, that is to say 1/50th of the pupil diameter. This result increase the uncertainty on the precision we can reach in laterally aligning the pupil with respect to a known reference on the scientific camera (using LBT ASM and tertiary mirror). Because of that, the current baseline for the pupil image alignment is to use a narrow band filter, representing the center of the wavelength range that will be used during the observation, to have a sharper image of the pupil onto the detector and being able to center it with a higher precision. Being the pupil image sampled with 390 pixel on a diameter, we expect that a SW routine could allow to define the center of the pupil, given the image, with a precision higher than 1 pixel, meaning about 0.2% of the pupil size. To account for pupil rotations, there might be two ways (both ok only for tracking between different exposures, not during):

- Add a pupil plane mask with "oversized" spiders, losing in throughput but being less sensitive to small mismatches between the real system geometry and the pupil plane mask
- Use the de-rotator, which is not foreseen for the planet finding mode, to adjust the rotation of the pupil image with respect to the masks, looking at the pupil image on the camera, once the deployable doublet is inserted. This would imply a calibration of the masks rotation angles with respect to the camera.

3.3 Minimization and characterization of the non-common path aberrations

The Non-Common Path Aberrations (NCPA) are minimized by design, being SHARK-NIR light, compact and positioned very close to the WFS. Direct measurements made with PISCES have shown a remarkably negligible amount of non-common path aberrations. Of course, they can be anyway characterized during daytime using a dedicated calibration source for LBTI. Additionally, an algorithm for the compensation of the pyramid variable gain with online measurement of the WFS sensitivity might be used to track the non-common path aberrations changes in almost real time. It will be possible to implement an optimizing routine to minimize the size of the PSF, introducing different amplitudes to a low number of modes (with a similar approach, to achieve a residual wavefront of the order of 20-30nm with FLAO-LUCI, the NCPA are minimized by looking at about 20 modes). At the moment, the baseline is to correct for non-common path aberrations with the ASM (the quality on the pyramid WFS obviously decreases, but recent studies show that the AO optimal performance can be retrieved also in this condition), however it has been considered the possibility of a future upgrade in which a local DM shall substitute the TT mirror. At the moment, we considered a commercial ALPAO DM suitable for this design, which is the DM 97-15, characterized by a pupil size of 13.5mm (the first re-imaged pupil size is 12mm of diameter), and having 97 actuators (actuator stroke of 40 to 60 microns), which we consider to be more than enough for the low order NCPA compensation.

3.4 Rejection of the quasi-static speckles

One of the major sources of noise limiting high-contrast imaging is caused by quasi-static speckles. Instrumental speckles (due mostly to optical quality and misalignment errors) average to form a fixed pattern, which can be calibrated to a certain extent, but their temporal evolution limits this possibility (for example because of mechanical and thermal deformation during the exposure). The ADI technique foreseen for exoplanets coronagraphic observation with SHARK, can minimize this effect. A sequence of images is acquired, normally with the telescope close to the Meridian, while the instrument field de-rotator is switched off. This keeps the instrument and telescope optics aligned and allows the field of view to rotate with respect to the instrument. For each image, a reference PSF is constructed from other appropriately selected images of the same sequence and subtracted to remove quasi-static PSF structures. All residual images are then rotated to align the field and are combined. Worth to be considered is also the technique of Principle Component Analysis[18] (PCA), an algorithm complementing ADI for increasing the contrast achievable next to a bright star. A possibility to quantify in advance the number of speckles and their power and temporal evolution would be to perform a forerunner experiment with a measurement campaign in the NIR band. In this framework, a possible approach would be to buy in an early stage the camera to be used as a TT sensor (sensitive to NIR) and take the opportunity to test it upgrading the VIS forerunner bench to NIR wavelenghts.

3.5 Out-of-pupil positioning of pupil masks

Due to the fact that in a coronagraph the source to be occulted is a point-like source in the center of the field, the angle over which the star is seen by the SHARK-NIR internal pupil images only depends on the angular size of the focused image delivered by the AO system. Thanks to that, the pupil apodizing masks leave a certain freedom in their positioning

along the optical axis. In the case of SHARK-NIR, this allows for the implementation of the local TT mirror, positioned on the pupil image, while the pupil mask is displaced. On the other hand, the maximum allowable displacement of the mask is related to the propagation effect of the rays moving away from the actual pupil, which decreases the achievable contrast. Combining the mentioned effect, the optimized position for SHARK-NIR apodizer has been chosen to be 50mm after the pupil plane, along the optical axis.

3.6 Throughput

3.6.1 Direct Imaging Mode

Table 2 reports a throughput budget (polychromatic, assuming a flat spectrum) which includes all the light-loss sources for the direct imaging mode. For the mirrors reflectivity, in particular, two different values have been considered (98% and 99%), since the final coating has not been selected yet.

Table 2 Throughput budget for the direct imaging mode

Item	Throughput contribution	Comments/remarks
Mirrors (OAPs, Flat and TT)	0.851	98% reflectivity assumed for each surface. 8 surfaces considered.
	0.923	99% reflectivity assumed for each surface. 8 surfaces considered.
Dewar window	0.97	
Detector	0.75	
TOTAL	0.62 to 0.67	
ADC	0.94	ADC shall be inserted for ZA>25deg
TOTAL (with ADC)	0.58 to 0.63	

The resulting throughput for the direct imaging mode is then between 58% and 67%, depending on the position on sky observed (for zenithal angles larger than ~25deg the ADC shall be inserted in the optical path) and on the reflectivity of the final coating adopted for the mirrors.

3.6.2 Coronagraphic mode

For the coronagraphic modes, instead, the final throughput is dominated by the pupil masks (apodizing and Lyot ones), as summarized in Table 3. In the case of classical Lyot, the throughput is reduced because of the undersizing of the pupil mask, which is, in our baseline, 90% of the full pupil image and with a central obscuration of 20%. Analogously, the mask placed on the second pupil image, for the Shaped Pupil case, is 98% of the full image and has a 12% central obscuration. In addition to that, the Shaped Pupil throughput is dominated by the apodizing mask (placed on the first pupil image), which allows only 30% of the light to reach the focal plane.

Table 3 Throughput budget for the coronagraphic modes

Item	w/o ADC		with ADC	
	Rcoating=99%	Rcoating=98%	Rcoating=99%	Rcoating=98%
Imaging mode throughput	0.67	0.62	0.63	0.58
Classical Lyot pupil stop	0.770			
Shaped Pupil masks effect	0.284			
Classical Lyot TOTAL	0.516	0.477	0.485	0.447
Shaped Pupil TOTAL	0.190	0.176	0.179	0.165

3.6.3 Spectroscopic modes

Finally, for the spectroscopic mode, the estimated throughput of the direct imaging shall be combined with a typical throughput of the dispersing elements. Here we explore both the prism case and the grism one. For the prism, the throughput is decreased because of two refractions (98% of trasmissivity each) and of the light loss inside the glass (assumed 1%). In the grism, instead, a typical throughput of ~60% is considered.

Table 4 Throughput budget for the spectroscopic modes

Item	w/o ADC		with ADC	
	Rcoating=99%	Rcoating=98%	Rcoating=99%	Rcoating=98%
Imaging mode throughput	0.67	0.62	0.63	0.58
Prism	0.95			
Grism	0.6			
Prism spectr. TOTAL	0.64	0.59	0.60	0.55
Grism spectr. TOTAL	0.40	0.37	0.38	0.35

3.7 Wavelenght trade-off

We estimated the cut-off frequency for the scientific image wavelength in order to minimize the thermal background, assuming a 180mm long baffle, positioned in front of the camera.

Table 5 The estimated thermal background varying the working temperature and the wavelength; the computation has been done considering a baffle 180mm long in front of the detector.

Temperature	Lambda (μm)	Photons per pixel per second
-10°C	1.60	<1
-10°C	1.65	~1
-10°C	1.70	~2
0°C	1.60	~2
0°C	1.65	~3
0°C	1.70	~5
+10°C	1.60	~5
+10°C	1.65	~8
+10°C	1.70	~15

The estimated thermal background is shown in Table 5. Considering a typical dit of 60s, the estimated thermal noise (Th_{noise}) can be computed as (Th_{noise}*60.)1/2, to be kept below the CCD expected readout noise, which is 15 e-/pix/readout (information taken from Teledyne technical specification). This comparison leads to a reasonable acceptable number of 4 to 5 photons per pixel per second. Considering also that most of the observations are carried out with temperatures around 0°C or below (from the data archived at LBT), the cut-off frequency of the H band shall be set to about 1.7μm, through a differential filter placed as close as possible to the detector.

3.8 Bearing de-rotation precision

Another issue to be addressed is the required precision for the de-rotation of the field, in order to compensate for the sky apparent rotation. If we consider as a requirement the need to have a stability of the PSF position (Δs, as defined in Figure 3) better than 0.25λ/D, for photometric purposes, then, assuming the worst case of a source positioned at the very corner of the CCD, the required precision in the field de-rotation is:

$$\Delta derot = \frac{0.25}{10.82} \cdot \frac{\lambda}{D} \cdot 206265^2 \cong 120'' \quad \text{(for } \lambda=1\mu m\text{)} \tag{1}$$

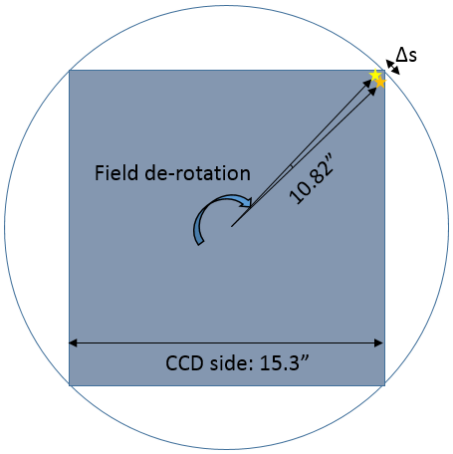

Figure 3 Effect of field de-rotation accuracy on the sources elongation at the edge of the FoV.

To reach this kind of stability in the field de-rotation, we shall assume a minimum incremental step smaller than about 1/5 of the required stability, that is to say <24". Another important parameter for the bearing selection is the maximum rotation speed needed. The maximum field de-rotation speed can be retrieved, given the minimum zenithal distance z and the site latitude L, with the following expression:

$$d\eta/dt = 0.262\, cosL/(sin\, z) \tag{2}$$

The mount Graham latitude is L=32.7°, while the nominal minimum zenithal distance for LBT is z =0.5°, resulting in a maximum rotation rate of 25.2rad/h = 24.1deg/min. Another limit in the allowable ZA can come from the maximum exposure time we want to exploit, which is of the order of 1h, combined with the maximum field de-rotation allowed by the de-rotator, which is 180deg.

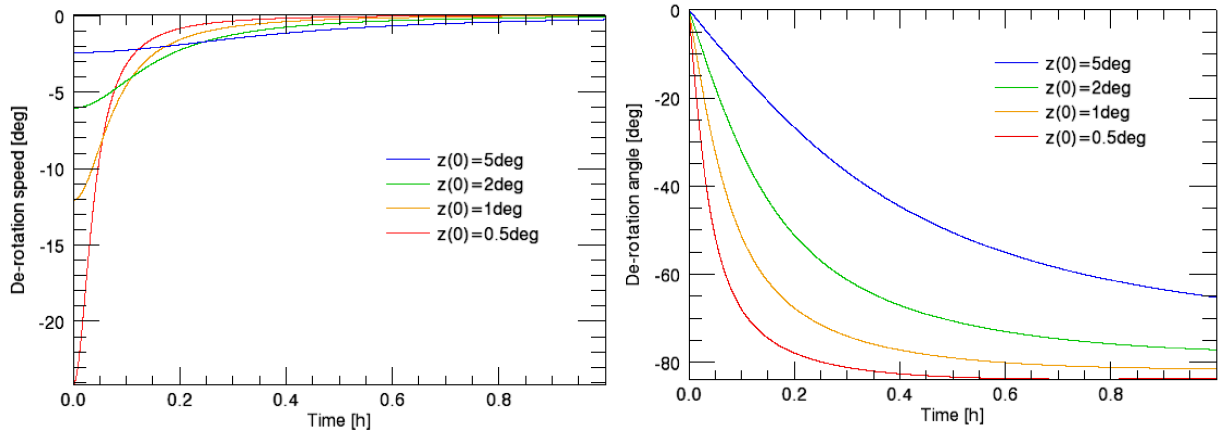

Figure 4 De-rotation speed and angle for object with different zenithal distance at transit.

Figure 4 reports the de-rotation speed and angle when following the trajectory of objects with different zenithal distance at the moment of transit. The graphs show that, if a given object transits through meridian with the minimum zenithal distance allowed by the telescope (0.5deg), a field de-rotation of less than 90 degrees is required in the first ½ hour after the transit. The de-rotator range, then, does not introduce any further limit to the zenithal angle. Of course, the computed maximum de-rotation speed is intended during a single exposure, and it is the speed for which the required precision (~120") shall be guaranteed. For technical/alignment issues a higher rotation speed (about two order of magnitude faster) shall be reached. In particular, the rotator should slew faster than the telescope (telescope azimuth moves at speeds up to 1.3 deg/sec, while gregorian rotator moves at 5 deg/sec) so that excess time is not spent when changing position angles.

3.9 Flexures

Despite being compact and light, the instrument will experience flexures during the change in elevation and during field de-rotation. Internally, on the SHARK-NIR bench, we do not expect flexures which are causing relative movements between the various components larger than the ones already simulated in the preliminary tolerance analysis, even considering going from zenith to ZA=65deg. In fact, internal movements due to flexures, considering the small bench dimension and the compact mounts, will rather give few microns of movements, and thus the effect on the optical quality (using as compensator the ASM static defocus term) should be negligible. On the other hand, the flexures of the overall instrument have been estimated in a preliminary flexures analysis as amounting to about +/- 100 microns of decenter and +/- 60" of tilt (the actual amount depending on the final way the instrument is attached to its interface, it could be reduce to the range +/-20 μm and +/- 10", changing the attaching points). However, these effects shall be compensated before each scientific exposure moving M2 and M3, in a way that they will not affect the optical quality inside SHARK-NIR.

4. ERROR BUDGETS

The budgets reported in the following include contributions from different sources of error, which are, at this phase of the project, partially estimated with analysis (with some assumptions) and partially guessed, according to experience with other systems.

4.1 Image stability onto the intermediate Focal Plane

Table 6 reports the preliminary budget for the Image stability onto the intermediate Focal Plane, where the occulter shall be placed. The following error sources have been considered:

- Calibration: for the PSF size/stability budget on the intermediate focal plane, we assumed a calibration tolerance, for the positioning of the star image onto the FP mask, of 10um.
- Flexures: we consider here only the effect of global flexures (of the whole SHARK-NIR bench with respect to the de-rotator), assuming a maximum flexure of 50μm at the entrance focal plane level, with respect to the bearing (this is an indicative value, as we said it will depend on the final mounting configuration – see also Section 3.9). This value will decrease if we only consider the effect during a single exposure. One has to consider the most probable elevation change required. Assuming the following expression for the elevation speed ZA'=0.25·cosL·sinA [deg/min], where ZA is the zenithal distance and L the site latitude, then we can consider a very conservative case, in which the elevation speed is ZA'=cosL=0.21 deg/min. If we assume a 1h observation, carried on when the object is crossing the meridian with the retrieved speed (constant, again, this is a very conservative case), then we obtain a maximum change in elevation of 0.21·30=6.3deg. We can then scale the flexure amount linearly (as a first order approximation), obtaining a ~5um shift on the intermediate FP. Of course, this is not the maximum possible elevation change during an exposure, but normally coronagraphic observations should be carried out around the meridian, to minimize the evolution of the quasi-static speckles. Anyway, even considering the maximum possible altitude change (15° per hour) the final impact on the error budget is the same, since this contribution is compensated through the slow rate TT correction.
- De-rotator wobble and runout: in this phase, we assume typical values that can be reached for a de-rotator with an analogous size and weight, which are about 10μm of runout and 10 μm of planarity of the reference surface, which translates (for a ~450mm wide bearing) to a wobble of about 0.01/450*206265=5".

- The assumed bearing runout and wobble are 20um and 15arcsec, respectively, for a full 180deg de-rotation. Considering all the possible observing modes, we must assume that the de-rotator can make a full 180deg rotation during an exposure. Considering the wobble, the effect of the tilt of the rays at the level of the entrance focal plane gives no image shift, while the SHARK-NIR entrance focal plane will experience a shift with respect to the LBT focal plane due to the leverage (~315mm) effect of the wobble occurring at the level of the bearing, estimated in about 33µm.
- AO residual jitter: discussed in Section 3.1.2
- Thermal effects: no detailed thermal analysis has been carried on either for the mechanics nor for the optical design. At the moment we consider the effect of a change in temperature on the relative positions of the optical elements, due to the bench expansion/contraction, given the steel CTE (about 12·10-6 ℃-1). As a first approximation this gives a shift of the image on the intermediate focal plane of 1.25um/degree. For this budget we estimated a change in temperature during a single observation lower than 2degrees.
- Tip-Tilt correction residual: some of the effects (the low-temporal-frequency ones) described above are going to be monitored using the local TT WFS and eventually corrected during the exposure with the local TT mirror. In our budget we have then to introduce a residual tip-tilt error, after the correction, estimated as lower than 5mas.

Table 6 Image stability on intermediate Focal Plane

	Tolerance during exposure	Unit	Shift @ intermediate FP (µm) – without TT correction	Shift @ intermediate FP (µm) – after TT correction
Calibration tolerances	10	µm	10	10
Flexures (whole SHARK-NIR bench)	5	µm	7.3	-
De-rotator runout	10	µm	14.6	-
De-rotator wobble	5	"	11.1	-
AO residual jitter	7	mas	6.16	6.16
Thermal effects	2.5	µm	2.5	-
TT correction residual	5	mas	-	4.4
TOTAL SHIFT (rms sum):			23.1 µm	12.5 µm

The budget is missing the effect of LBT flexures, but they will be in any case included in the wavefront error (WFE) to be corrected with the local TT mirror, thanks to the local TT WFS monitoring. The result of this budget is ~12.5 µm, which shall be compared with the image shift allowed by the most sensitive coronagraphic technique implemented. If we consider the smallest occulter to be placed in the intermediate focal plane filter wheel, that is to say a mask designed to allow for Inner Working Angle ~2λ/D in J band, that would have a diameter of about 88µm. In the exo-planets scientific case, the contribution of the bearing to the motion of the image on the focal plane shall not be considered, since in the ADI coronagraphic mode the field is not de-rotated.

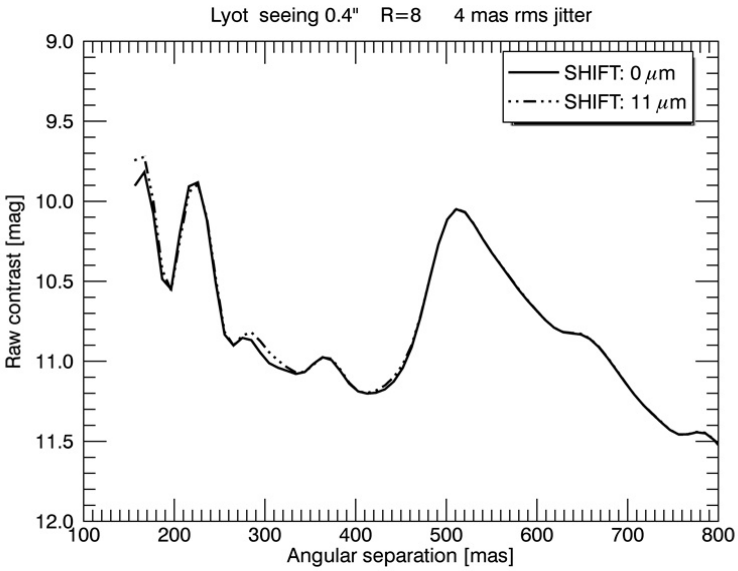

Figure 5 Effect of a shift of the occulting mask in the classical Lyot case, in good seeing conditions, for a bright source.

The final degradation we are interested into regards the contrast parameter. To estimate the effect a simulation has been performed, assuming a shift of the occulter of an amount which is comparable with the result of our budget (11um, excluded the jitter, which has been simulated directly on the incoming wavefronts). Figure 5 shows that this kind of lateral shift of the image on the intermediate focal plane results into a decrease in the raw contrast which is basically negligible.

4.2 Strehl Ratio on the scientific Focal Plane

Table 7 reports the preliminary budget for the SR obtained onto the final scientific Focal Plane, where the NIR camera is placed. We here considered the expected SR in the circular field inscribed in the detector, that is to say a FoV with a 15.3" diameter. The following error sources have been considered:

- Nominal optical design: the nominal SR is 99% SR (@1μm).
- Alignment: a preliminary alignment tolerance analysis has been carried on, resulting in a performance decrease from 99% SR to about 0.98% SR (@1μm) with respect to the nominal design. The contribution of the alignment in the WFE budget is then about 0.1rad, after we removed in quadrature the rms WFE of the nominal design.
- ADC: the effect of the ADC on the on-axis performance results in a SR decrease to about 0.98% @ZA=50deg and 0.96.5% @ZA=60deg (@1μm). In the budget we considered the conservative but not worst case of the ZA=50deg, after we removed in quadrature the rms WFE of the nominal design. It shall be noticed that the contribution for lower zenithal angles is almost negligible (nominal optical quality is reached for ZA<30deg).
- Flexures: flexures have been estimated as we already explained in Section 4.1.
- De-rotator wobble and runout: effects due to the de-rotator have been estimated as we already explained in Section 4.1.
- De-rotator angular accuracy: described in Section 3.8.
- Thermal effects: the same assumption made in Section 4.1 has been done, resulting in an overall defocus at the level of the NIR detector of slightly less than 100μm.
- NCPA: another possible source of error are the Non Common Path aberration, which will be corrected with the ASM (see Section 3.3), but the correction will leave a residual WFE, depending on how the characterization is

made. As reported in Section 3.3, at the moment, the estimated (obtained with FLAO-LUCI, using an analogous algorithm for characterization) residual WFE is of the order of 20-30nm.

- Tip-tilt correction residual: see Section 4.1.

The budget is missing the effect of LBT flexures.

Table 7 WFE on the scientific Focal Plane

	Tolerance during exposure	Unit	WFE (nm) - without TT correction	WFE (nm) - after TT correction
Optical design (nominal)			16	16
Alignment tolerances			16	16
ADC (@ZA=50deg)			16	16
Flexures (full SHARK)	5	µm on entrance FP	55	-
De-rotator runout	10	µm on entrance FP	110	-
De-rotator wobble	5	“	84	-
De-rotator angular accuracy	24	”	0.2	0.2
Thermal effects			23	-
NCPA aberration	20	nm WFE	20	20
TT correction residual	5	mas	-	13
TOTAL WFE (rms sum):			155	47.5
RESULTING SR(J):			54%	94%
RESULTING SR(H):			71%	97.0%

We want here to stress that, despite missing second order contributions, the budget shown here is a very conservative one, since it does not include median values and in some cases large margins have been taken. This choice is mainly due to the fact that the full analysis has not yet been performed at this level of the system design, being some inputs still missing (NCPA and TT correction residual). As said in the previous paragraph, in the exo-planets scientific case, the contribution of the bearing to the smearing of the image on the focal plane shall not be considered, since in the ADI coronographic mode the field is not de-rotated. The budget in Table 7 reports the intrinsic SR (the one only due to SHARK-NIR) in different wavelength bands. To translate this into a coronagraphic contrast we shall combine also the quality of the PSF delivered by FLAO onto the SHARK-NIR entrance focal plane (LBT F/15 focal plane). This quality can be separated into two contribution: the short-exposure PSF and the residual jitter (see Section 3.1.2). The WFE due to the first term can be retrieved from the residuals data cubes we received from the FLAO team and used as inputs in our simulations[17]. The value depends on the seeing conditions and on the reference source brightness. The effect of the AO residual jitter can be estimated, as a first approximation, introducing an ad-hoc tip-tilt to the incoming wavefronts. The values reported in Table 8 assume a sinusoidal variation of the tip-tilt value during one exposure (conservative).

Table 8 Possible performance delivered by FLAO, depending on the short-exposure PSF and on the residual jitter.

Short-exposure PSF SR@H / AO residual jitter (rms)	95%	90%	85%	80%
2 mas	94.4%	89.5%	84.5%	79.5%
4 mas	92.8%	88.0%	83.1%	78.2%
8 mas	86.7%	82.1%	77.5%	73.0%
16 mas	65.8%	62.3%	58.9%	55.4%

The effect of the SR decrease described in the error budget will be translated into coronagraphic contrast performance on a later stage, when the space of parameters used for the simulations in different observing conditions (magnitude vs seeing vs jitter vs coronagraphic technique) will be more complete.

REFERENCES

[1] Hill, J. M. and Salinari, P., "Large Binocular Telescope project," Proc. SPIE, 4004, 36–46 (2000).

[2] Esposito, S., Riccardi, A., Pinna, E., Puglisi, A. T., Quirós-Pacheco, F., Arcidiacono, C., Xompero, M., Briguglio, R., Busoni, L., Fini, L., Argomedo, J., Gherardi, A., Agapito, G., Brusa, G., Miller, D. L., Guerra Ramon, J. C., Boutsia, K. and Stefanini, P. "Natural guide star adaptive optics systems at LBT: FLAO commissioning and science operations status," in Proc. SPIE, 8447, 84470U (2012)

[3] Ragazzoni, R., "Pupil plane wavefront sensing with an oscillating prism," Journal of Modern Optics 43, 289 (1996).

[4] Farinato, J., Pedichini, F., Pinna, E., Baffa, C., Baruffolo, A., Bergomi, M., Carbonaro, L., Carolo, E., Carlotti, A., Centrone, M., Close, L., De Pascale, M., Dima, M., Esposito, S., Fantinel, D., Farisato, G., Gaessler, W., Giallongo, E., Greggio, D., Guyon, O., Hinz, P., Lisi, F., Magrin, D., Marafatto, L., Puglisi, A., Ragazzoni, R., Salasnich, B., Stangalini, M., Vassallo, D., Verinaud, C. and Viotto, V., "SHARK-NIR: From K-band to a Key instrument... A status update," in Proc. SPIE, (this conference)

[5] Farinato, J., Baffa, C., Baruffolo, A., Bergomi, M., Carbonaro, L., Carlotti, A., Centrone, M., Codona, J., Dima, M., Esposito, S., Fantinel, D., Farisato, G., Gaessler, W., Giallongo, E., Greggio, D., Hink, P., Lisi, F., Magrin, D., Marafatto, L., Pedichini, F., Pinna, E., Puglisi, A., Ragazzoni, R., Salasnich, B., Stangalini, M., Verinaud, C. and Viotto, V., "The NIR arm of SHARK (System for coronagraphy with High order Adaptive optics from R to K band)," International Journal of Astrobiology, 14(3), 365-373 (2015)

[6] Lyot, B., "The study of the solar corona and prominences without eclipses," Monthly Notices of the Royal Astronomical Society, 99, 580 (1939).

[7] Kuzuhara, M., Tamura, M., Kudo, T., Janson, M., Kandori, R., Brandt, T. D., Thalmann, C., Spiegel, D., Biller, B., Carson, J., Hori, Y., Suzuki, R., Burrows, A., Henning, T., Turner, E. L., McElwain, M. W., Moro-Martín, A., Suenaga, T., Takahashi, Y. H., Kwon, J., Lucas, P., Abe, L., Brandner, W., Egner, S., Feldt, M., Fujiwara, H., Goto, M., Grady, C. A., Guyon, O., Hashimoto, J., Hayano, Y., Hayashi, M., Hayashi, S. S., Hodapp, K. W., Ishii, M., Iye, M., Knapp, G. R., Matsuo, T., Mayama, S., Miyama, S., Morino, J.-I., Nishikawa, J., Nishimura, T., Kotani, T., Kusakabe, N., Pyo, T.-S., Serabyn, E., Suto, H., Takami, M., Takato, N., Terada, H., Tomono,

D., Watanabe, M., Wisniewski, J. P., Yamada, T., Takami, H. and Usuda, T., "Direct Imaging of a Cold Jovian Exoplanet in Orbit around the Sun-like Star GJ 504," The Astrophysical Journal, 774, 11 (2013)

[8] Hinz, P.M., Angel, J.R.P., McCarthy, D.W., Hoffman, W.F., and Peng, C.Y., "The large binocular telescope interferometer," in Proc. SPIE, 4838, 108 (2003).

[9] Wilson, J.C., Hinz, P.M., Skrutskie, M.F., Jones, T., Solheid, E., Leisenring, J., Garnavich, P., Kenworthy, M., Nelson, M.J., and Woodward, C.E., "LMIRcam: an L/M-band imager for the LBT combined focus," in Proc. SPIE, 7013, 101 (2008).

[10] Macintosh, B.A., Graham, J.R., Palmer, D.W., Doyon, R., Dunn, J., Gavel, D.T., Larkin, J., Oppenheimer, B., Saddlemyer, L., Sivaramakrishnan, A., Wallace, J.K., Bauman, B., Erickson, D.A., Marois, C., Poyneer, L.A., and Soummer, R. "The Gemini Planet Imager: from science to design to construction," in Proc. SPIE, 7015, 31 (2008).

[11] Beuzit, J.-L., Boccaletti, A., Feldt, M., Dohlen, K., Mouillet, D., Puget, P., Wildi, F., Abe, L., Antichi, J., Baruffolo, A., Baudoz, P., Carbillet, M., Charton, J., Claudi, R., Desidera, S., Downing, M., Fabron, C., Feautrier, P., Fedrigo, E., Fusco, T., Gach, J.-L., Giro, E., Gratton, R., Henning, T., Hubin, N., Joos, F., Kasper, M., Lagrange, A.-M., Langlois, M., Lenzen, R., Moutou, C., Pavlov, A., Petit, C., Pragt, J., Rabou, P., Rigal, F., Rochat, S., Roelfsema, R., Rousset, G., Saisse, M., Schmid, H.-M., Stadler, E., Thalmann, C., Turatto, M., Udry, S., Vakili, F., Vigan, A., and Waters, R. "Direct detection of giant extrasolar planets with SPHERE on the VLT," Astronomical Society of the Pacific workshop Proc., 430, 231 (2010).

[12] Soummer, R., "Apodized Pupil Lyot Coronagraph for Arbitrary Telescope Apertures," The Astrophysical Journal, 618, 161 (2005)

[13] Carlotti, A., Kasdin, N.J., Vanderbei, R.J., and Delorme, J-R., "Optimized shaped pupil masks for pupil with obscuration," in Proc. SPIE, 8442, 54 (2012).

[14] Ren, D., Dou, J., Zhang, X., and Zhu, Y., "Speckle noise subtraction and suppression with adaptive optics coronagraphic imaging," Astrophysical Journal, 753, 99 (2012).

[15] Riccardi, A. Xompero, M., Briguglio, R., Quirós-Pacheco, F., Busoni, L., Fini, L., Puglisi, A., Esposito, S., Arcidiacono, C., Pinna, E., Ranfagni, P., Salinari, P., Brusa, G., Demers, R., Biasi, R., and Gallieni, D., "The adaptive secondary mirror for the Large Binocular Telescope: optical acceptance test and preliminary on-sky commissioning results," in Proc. SPIE, 7736, 79 (2010).

[16] Pinna, E., Pedichini, F., Farinato, J., Esposito, S., Centrone, M., Puglisi, A., Carbonaro, L., Agapito, G., Riccardi, A., Xompero, M., Hinz, P., Montoya, M., and Bailey, V., "XAO at LBT: current performances in the visible and upcoming upgrade," Proc. of forth AO4ELT conference, (2015).

[17] Vassallo, D., Carolo, E., Farinato, J., Bergomi, M., Bonavita, M., Carlotti, A., Greggio, D., Magrin, D., Mesa, D., Pinna, E., Puglisi, A., Stangalini, M., Verinaud, C., and Viotto, V., "An extensive coronagraphic simulation applied to LBT," in Proc. SPIE, (this conference).

[18] Meshkat, T., Kenworthy, M. A., Quanz, S. P., and Amara, A., "Optimized Principal Component Analysis on Coronagraphic Images of the Fomalhaut System", The Astrophysical Journal, 780, 17 (2014)